Evaporation Studies of the Metals and Alloys Used in the TEMPUS Flight Experiments

Kin F. Man, Pramod K. Sharma, Gregory S. Hickey and John L. Watkins

Jet Propulsion Laboratory
California Institute of Technology
4800 Oak Grove Drive
Pasadena, CA 91109

Abstract

Evaporation rates have been measured for the metals and alloys to be used in the TEMPUS flight experiments (except for Zr) in order to facilitate a rational assignment of a flight sequence that will minimize the effects of particulate and cross contamination. The samples were melted in a crucible by electron beam heating to temperatures 30 to 300 ʻC above their melting point. The evaporation rates were obtained from measurements of sample weight-loss during processing and by analysis of the film deposited on metal foils. A model has been developed for calculating the evaporation rates for multi-component alloys based on vapor pressure contributions of each component in the alloy system. The theoretical predictions show good agreement with the experimental results in the majority of cases, some within a factor of two. In a few cases, significant differences were observed. These were mainly attributed to uncertainties in the input vapor pressure data.

1. Introduction

A number of metals and alloys have been selected for microgravity experiments involving nucleation, undercooking, viscosity, surface tension, non-equilibriurn solidification, and thermodynamic studies in the TEMPUS [1] facility (an electromagnetic positioning system scheduled to be flown as part of the IML-2 mission in mid-1994 aboard the Space Shuttle). All experiments involve heating the material samples above their melting point while being positioned with water-cooled copper electromagnetic coils in ultrahigh vacuum or in an inert gas atmosphere. A molten sample maintained at high temperature will continuously evaporate and coat all the surfaces within its line of sight, including the nearby copper coils. Depending on how the deposited material sticks to the copper coils and the thickness of the deposited film, some of the evaporated material may come off the coils as particulate. In the microgravity environment, they will float around in the experimental chamber without gravity to settle them to the bottom. These particulate can act as heterogeneous nucleation sites for nucleation experiments, as impurities in undercooking experiments that would prevent deep undercooking, or as disturbing factors in the thermophysical properties measurements that would increase the experimental errors. The higher the rate of evaporation a sample has, the more likely it is for particulate to come off the surfaces (if all other factors remain the same).

In order to assess the potential problem due to particulate generation of the evaporated materials from surfaces, it is necessary to know the evaporation rate for each sample. The rate of evaporation of a material is directly related to its vapor pressure at a given temperature. By knowing the vapor pressure, the evaporation rate can be estimated. Unfortunately, not all vapor pressure data for the materials of interest are available, especially at or above their melting point. For those data that are available, in some cases reported values of the same quantity may differ by orders of magnitude.

In the present study, the evaporation rates of the metals and alloys to be used in TEMPUS have been measured to assess the likely potential problems due to particulate contamination and to facilitate a rational assignment of a flight sequence that would minimize the problems of particulate and cross contamination. The experimental set up used in the evaporation rate measurement and the different methods used for obtaining the evaporation rates from the experimental

measurements are described in section 2. A model for calculating the evaporation rates for multi-component alloys based on vapor pressure contributions of each component in the alloy system has been developed. In sections 3 and 4, the model and the results of some typical calculations are briefly described, so that alloy systems of a different composition can be readily calculated. Comparisons of the experimental and theoretical results and discussions of these results are given in section 5.

2. **Experimental**

A schematic diagram of the experimental setup for measuring evaporation rate of metals and alloys is shown in Fig. 1. The sample to be investigated was put inside a crucible of a non-reactive inert material. The crucible was inserted into an electrically conductive molybdenum cup for electron beam heating by a 1.5 turn tungsten filament coil. The temperature of the sample was measured by a tungsten—tungsten-rhenium (W/WRe) thermocouple attached to the bottom of the Mo cup. The crucible structure was supported by a tantalum dish and a thin-wall tube to minimize conductive heat loss. The Ta tube was also used to shield the bare thermocouple wires from electron bombardment which would cause temperature fluctuations. Two thin stainless steel foils were placed above the sample at a known distance (about 3 inches) away from the crucible to collect the evaporated material. There was also a quartz microbalance film thickness monitor with a direct line of sight to the molten sample for measuring the film thickness as the temperature increased. (Unfortunately, the microbalance failed when the temperature of the crucible structure exceeded about 800 °C. The radiation apparently overheated the monitor and its electronics, despite water-cooling.) The whole setup was housed in a vacuum chamber that could be evacuated to a base pressure of high 10^{-9} torr by a turbomolecular pump.

2.1 **Material Samples**

Most of the samples were prepared at the California Institute of Technology [2] and some were provided by the Principal Investigators. They were made by one of three methods, electromagnetic heating in a silver boat, plasma arc melting and induction heating in a glass container. A list of the materials and their melting temperatures are shown in Table 1.

The metal and alloy samples were cleaned by etching in dilute nitric acid to remove the oxide film on the surface and rinsed in pure ethanol to remove any residual acid. They were then weighed, put into a crucible and quickly transferred to the vacuum chamber.

2.2 **Crucibles**

Three types of crucible materials were used in the experimental measurements, boron nitride, alumina (both 1/2" o.d., 3/8" id., 1/2" height) and zirconium oxide (3/8" o.d., 9/32" id., 1/2" height). Many considerations were taken into account in the selection of these crucibles: Reactivity with the metals and alloys to be studied, wetting of the molten samples on the surfaces, thermal shock, melting temperature, and vapor pressure at the melting temperature of the sample. Zirconium oxide crucibles have the highest melting point and the lowest reactivity at a given temperature, so they are generally preferred over the other two materials. But zirconium oxide crucibles were used only for the higher melting materials (Ni and Fe75-Ni25) because they were not readily available. Boron nitride and alumina crucibles were therefore used for most of the experiments. Since boron nitride is hydroscopic, they were prebaked at 400 °C for 15 hours in a low vacuum and stored in a desiccator until use.

2.3 **Heating**

Heating was provided by an electron beam with a fixed -4kV high voltage and a variable electron beam current of 10 to 150 mA. There was a slight drift in electron current, due to instability in the power supply, which caused a small drift in temperature. Constant adjustments were made to stabilize the temperature. The error in the experimental results reflects this temperature drift.

2.4 **Temperature Measurement and Calibration**

The temperature was measured with a W/WRe thermocouple attached to the bottom of the Mo cup (see Fig. 1). Since there was a temperature gradient between the bottom of the Mo cup and the sample in the crucible, heating was increased very slowly to maintain a steady state and the temperature gradient was obtained by noting the thermocouple reading at the initial sample melting compared with its true melting

temperature. The error in the experimental results also reflects some of this uncertainty in the temperature measurement.

2.5 **Evaporation Rate Determination**

The evaporation rate was determined by three different methods that served as cross checks to verify the accuracy of the measurements:

1. Weight-loss method — the sample and crucible were weighed before and after heating at a specified temperature for a specified time. The difference in weight was used to calculate the evaporation rate at a certain temperature and time for a given sample size.
2. Weight-gain method — the foils (stainless steel, 0.5" dia., 0.002" thick) located above the crucible were weighed before and after heating at a specified temperature for a specified time. The gain in weight from the evaporated material was used to calculate the evaporation rate at a certain temperature and time for a given foil size.
3. SEM method — the film thickness of the foils was measured at the end of the experiment by Scanning Electron Microscopy (SEM). For materials with low evaporation (and therefore extremely low total sample weight-loss or weight-gain on the foils) SEM analysis was the only method of obtaining an accurate evaporation rate.

2.6 **Evaporation Geometry and Total Mass Loss**

In order to obtain the rate of evaporation, the total mass evaporated from the sample has to be calculated from a knowledge of the weight-gain or film thickness on the foils. This in turn requires a knowledge of the evaporation geometry. Fig. 2 shows the geometry used to obtain the total evaporated area at a distance H from the sample.

Emission from a source of finite dimension into a vacuum chamber follows a cosine distribution. Thus, the evaporation onto a flat surface located above the crucible is likely to follow a similar distribution. However, in our experimental setup the angle subtended by the foils was small (less than 25°), so it was assumed that the emission reaching the center of the surface was very similar to that reaching the periphery. I-his assumption may introduce a maximum error of about 9'% ($\cos 25^\circ = 0.91$). It is further

6

assumed that there is minimal re-emission of the evaporated material from the inside wall surfaces of the crucible.

With the above simplifying assumptions, the total mass of material, M, evaporated and lost from a sample of a given size is simply given by:

$$M = \alpha A \rho$$

where

α = film thickness obtained by SEM

A = area of deposition subtended by the sample (Fig. 2)

ρ = density of the evaporated material. For alloys with significant vapor pressure contributions from more than one component, a weighted average density was taken

For materials with high evaporation and therefore a measurable weight gain on the foil, the total evaporated mass, M, was obtained from:

$$M = Am/a$$

where

m = weight gained on the foil

a = surface area of the foil

For high evaporation rate materials that had a significant total sample weight loss and measurable weight gain on the foils, the mass loss/gain obtained by the above methods agreed to within 30% for many samples and all of them agreed to better than a factor of 2. In all cases the weight loss values obtained from the different methods were averaged,

2.7 **Evaporation Rate Calculations**

The evaporation rate, R, is calculated from the following:

$$R == M/A_s t$$

where

M = total mass loss obtained from section 2.6

A_s = emitting surface area of the sample, obtained from direct measurement of the sample surface area after the experiment. For samples that did not stick to the crucible we took half the spherical area as the total emitting surface area

t = total evaporation time at a given temperature

3. A Model for Material Evaporation

A model to predict the evaporation rate of metallic melts was developed. It assumes a spherical molten drop evaporating into an ultrahigh vacuum.

First, consider the interface at the surface of the melt (see Fig. 3). For simplicity, assume that the interface is thin enough that the evaporating species pressure at the interface is the same [3] as its vapor pressure. Further assume that the environment just outside the interface is a perfect vacuum so that molecules can leave the interface because of its vapor pressure (thus causing sample evaporation), but they cannot enter the interface from the outside.

The flux of molecules (or atoms of a monatomic vapor) leaving a unit area at the interface is given, from kinetic theory [4], as:

$$\text{number flux} = 1/4 \ n \ v_{av} \quad \text{molecules/cm}^2\text{-sec} \tag{1}$$

where n is the number density and v_{av} is the average molecular velocity for the evaporating species, which is related to the root-mean-square velocity by:

$$v_{av} = v_{rms}/1.086 \tag{2}$$

where the root-mean-square velocity is given as:

$$v^2_{rms} = 3 \, k \, T / m \tag{3}$$

where k is the Boltzmann constant, T is the absolute temperature, and m is the molecular mass.

The number density n forthevapor isrelated tothevapor pressure by:

$$n = N \, p_g / RT \tag{4}$$

where p_g is the vapor pressure of the evaporating species at temperature T. For most metals, the vapor pressure varies with temperature according to a linear relationship between ln (p_g) and l/T.

3.1 Pure Metals

The computation of evaporation rates of pure metals is carried out directly from the above relationships. This requires vapor pressure data in the desired temperature range, The majority of data used in this analysis for pure metals were compiled by Samsonov [5] and Smithells [6]. The data for nickel were obtained from thermodynamic calculations (Heats of Formation and Free Energy from JANAF Tables [7]). In all cases, the values between data points were interpolated by curve fitting with an appropriate polynomial.

3.2 Alloys

For alloys of two or more components, the above relationships, with some modifications from a single to a multicomponent mixture, can be used. The total vapor pressure of the mixture is then the sum of the individual component partial pressures.

In general, the partial pressure of a component of mole fraction χ in the liquid state can be expressed as:

$$P = \gamma \cdot \chi \cdot p^o_g \tag{5}$$

where γ is the activity coefficient of the component in the liquid phase and p^o_g is the vapor pressure of the pure component. The activity coefficient y takes into account the nonidealities of the solution and, in the case of an ideal solution, it is equal to unity.

For simplicity, we assume ideal solutions in the liquid state. With the coefficient $\gamma = 1$, the component partial pressure given by the above equation reduces to Henry's law. The individual component vapor pressure can now be computed as:

$$p_{g1} = p^o_{g1} \cdot \chi_1 \tag{6}$$

where p_{g1} is the partial pressure of component 1, p^o_{g1} is the vapor pressure of pure component 1, and χ_1 is the mole fraction of component 1 in the liquid phase. Therefore, the total pressure of the mixture with three components (mole fractions χ_1, χ_2, and χ_3) can be written as:

$$p_g = p^o_{g1} \cdot \chi_1 + p^o_{g2} \text{``} \chi_2 + p^o_{g3} \text{``} \chi_3 \tag{7}$$

By knowing the individual component partial pressures in the vapor phase and the total vapor pressure of the mixture, one can obtain the component mole fractions in the vapor phase χ_{g1}, χ_{g2}, and χ_{g3}.

The average number density in the vapor phase can then be estimated from Equation (4), and the average molecular mass for the vapor mixture can be estimated to be:

$$m = m_1 \cdot \chi_{g1} + m_2 \cdot \chi_{g2} + m_3 \cdot \chi_{g3} \tag{8}$$

The evaporation rate from the melt in a vacuum environment is computed by converting the number flux into the mass flux.

4. Computation of Evaporation Rates

The computation of evaporation rates of metals and alloys is illustrated here for the Urban 1 sample, a ternary alloy system, at a temperature of 965 ^oC. The weight percent (wt %) composition of this alloy is Al(60)-Cu(34)-Fe(6).

By converting from wt % to mole %, the alloy composition can be expressed as Al(77)-Cu(19)-Fe(4), with component mole fractions $\chi_{Al} = 0.77$, $\chi_{Cu} = 0.19$, and $\chi_{Fe} = 0.04$. The pure component vapor pressures at this temperature are [5, 6, 7] $p^o_{Al} = 6.14 \times 10^{-5}$ torr, $p^o_{Cu} = 8.40 \times 10^{-5}$ torr, and $p^o_{Fe} = 3.37 \times 10^{-7}$ torr.

According to Equation (6), the individual component vapor pressures in the molten alloy are $p_{g_{Al}} = 4.79 \times 10^{-5}$ torr $= 6.28 \times 10^{-8}$ atm, $p_{g_{Cu}} = 1.60 \times 10^{-5}$ torr $= 2.05 \times 10^{-8}$ atm, $p_{g_{Fe}} = 1.35 \times 10^{-8}$ torr $= 1.77 \times 10^{-11}$ atm. The total vapor pressure of the melt is then given as the sum of the individual component vapor pressures, $p_g = 8.33 \times 10^{-8}$ atm. The number density, n, is now obtained from Equation (4) using N $= 6.023 \times 10^{23}$ molecules/g-mole, T $= 1238$ K, R $= 82.0$ $cm^3 \cdot$atm/gmole-K, and the vapor pressure values given above. This gives n $= 4.94 \times 10^{11}$ molecules/cm^3.

From Equation (9), the average molecular mass in the vapor phase is calculated to be m $= 5.98 \times 10^{-23}$ g/molecule and the average molecular velocity is obtained from Equations (2) and (3) to be $v_{av} = 8.52 \times 10^4$ cm/sec. The number flux of the evaporating molecules can now be obtained from Equation (l), number flux = 1.05 $\times 10^{16}$ molecules/cm^2-sec. The mass flux for the evaporating molecules (or the evaporation rate per unit surface area) is obtained by multiplying the number flux by the average molecular mass, evaporation rate:- 6.29 x 10-7 g/cm^2-sec.

5. Results and Discussion

The measured evaporation rates and experimental conditions are tabulated in Table 1. The temperatures ranged from about 30 to 300 *C above their melting point. The vacuum levels in the experimental chamber were mostly in the 10^{-6} and 10^{-7}torr range. The duration of evaporation depended on the evaporation rate and for materials with low evaporation the sample was evaporated for more than three hours to obtain an accurate measurement.

Table 2 shows a comparison between the experimental measurements and theoretical calculations. There is good agreement between the measured and predicted evaporation rates (within a factor of 3) for about 10 of the results. For another 10 of the cases, the measured and predicted values are within an order of magnitude. For the remaining 6 cases, the agreements are poor and the differences between the measured and predicted values exceed a factor of 10. There are several reasons for the differences between the measured and predicted evaporation rates. l-he fact that the model predictions were based on a perfect vacuum whereas the vacuum chamber pressures were in the range of 10^{-5} to 10^{-7} torr during the measurements may have partly accounted for the predicted values to exceed the measured values in some cases. Another source of significant error in the predictions is the input vapor pressure

(as a function of temperature) for each component. Finally, the non-ideality of the solution (or the melt) will also affect the component vapor pressures. These sources of error, when combined, may account for a factor of 2 to 3 difference between the measured and predicted evaporation rates. While the measurements reported here may not yield component vapor pressures with high precision, but when deviations exceed a factor of 3 they do indicate that the input vapor pressures of the individual components are somewhat suspect.

6. **Acknowledgments**

7. **References**

1. **G.** Lohofer, P. Neuhaus and 1. Egry, High Temp. High Pressure 23, 333 (1991)

2. The samples prepared at the California Institute of Technology were by David Lee.

3. Treybal, R. E., "Mass Transfer Operations," McGraw-Hill, London (1 **968).**

4. **See,** for example, Present, R. D., Kinetic Theory of Gases, McGraw-Hill, New York (1 958) p.33.

5. Samsonov, G. V., editor, Handbook of the Physicochemical Properties of the Elements, Plenum Press, New York (1968) pp. 252-258.

6. Smithells, C. J., cd., Metals_ Reference Book, Butterworths, London (1 976).

7. JANAF Thermochemical Tables, 3rd edition, J. of Physical and Chemical Reference Data, Vol. 14 (1985), Supplement No. 1

8. Table Captions

1. Evaporation rate measurements at different temperatures, chamber vacuum level and evaporation time for the metals and alloys used in TEMPUS.

2. A comparison of the experimental and theoretical evaporation rates of the metals and alloys used in TEMPUS.

9. Figure Captions

1. Experimental apparatus for evaporation rate measurements.

2. Geometry used for obtaining the evaporated area in the calculation of evaporation rate from film thickness measurements.

3. Simple model showing an evaporating sphere.

Table 1. Evaporation rate measurements at different temperatures, chamber vacuum level and evaporation time for the metals and alloys used in TEMPUS.

FO#	FO	Material Sample	Evap. Rate R (g/cm^2.s)	Temp (°C)	Vac.Lev. (Torr)	Evap.Time T(min)
2	Urban 1	Al60-Cu34-Fe6	$(2.16\pm1.58)\times10^{-7}$	965$\pm$10	4.0x10^{-7}	120
3	Egry 1	Au	$(5.22\pm1.30)\times10^{-6}$	1124$\pm$10	4.5X10^{-6}	38
4	Egry 3	Au	$(5.22*1.30)\times10^{-6}$	1124$\pm$10	4.5 X1 O-6	'3 8
5	Flemings 1	Ni75-Sn25	Spitted (in BN crucible)	1275$\pm$10	6.0x10^{-6}	53
			$(3.56\pm1.78)\times10^{-6}$ (in AO crucible)	1285110	1.2 X1 O-6	78
6	Szekely 1	Au56-Cu44	$(1.04\pm0.26)\times10^{-6}$	1075*1 o	1.5 x10^{-6}	104
7	Flemings 3	Ni67.5-Sn32.5	$(1.31\pm0.65)\times10^{-6}$	1192$\pm$10	4.0x10^{-6}	50
8	Szekely 4	Cu	$(3.46\pm0.86)\times10^{-5}$	1123110	1.3 X1 O-5	30
9	Herlach 3	Ni79-Si21	$(4.06\pm2.03)\times10^{-7}$	1224$\pm$10	I, OX1O-6	134
10	Fecht 1	Zr64-Ni36	$(2.21\pm0.55)\times10^{-8}$	1 090$\pm$1o	6.0x10^{-7}	185
11	Fecht 2	Zr76-Fe24	$(1.00\pm0.50)\times10^{-7}$	1018$\pm$15	1. OX1O-6	180
12	Johnson 4	Ni59.5-Nb40.5	$(3.72*1.86)\times10^{-6}$	1370il 5	2. OX1O-5	81
			$(2.27\pm0.56)\times10^{-7}$	1225$\pm$10	1.5x10^{-6}	[35
13	Bayuzick 2	Zr	Not measured			
14	Urban3	Al65-Cu25-Co1O	$(1.14\pm0.57)\times10^{-6}$	1050$\pm$10	3.5 X1 O-7	60
15	Szekely 3	Au56-Cu44	$(1.04\pm0.26)\times10^{-6}$	1 075$\pm$1o	1.5x10^{-6}	-i 04
16	Flemings 4	Ni67.5-Sn32.5	$(1.31\pm0.65)\times10^{-6}$	1192$\pm$10	4.0x10^{-6}	50
17	Johnson 3	Zr76-Ni24	$(7.24\pm1.81) \times10^{-8}$	1100$\pm$15	1.0x10^{-6}	170
			$<(4.7831.? O) \times10^{-9}$	1055$\pm$10	8.0x1 0^{-7}	120
18	Fecht 3	Zr78.5-Co21.5	$<(2.76\pm1.38)\times10^{-9}$	1082$\pm$15	5. OX1O-7	166
19	"Urban 2	Al67-Cu21-Co12	$(4.88\pm2.44)\times10^{-5}$	1320315	3.0x10^{-6}	13
			$(7.28\pm3.64)\times10^{-7}$	1090$\pm$1o	5.0x10^{-7}	72
20	Flemings 2	Ni75-Sn25	Spitted (in BN crucible)	1275$\pm$10	6.0x10^{-6}	53
			$(3.56\pm1.78)\times10^{-6}$ (in AO crucible)	1285$\pm$1O	1.2 X1 O-6	'7 8
21	Herlach 1	Fe75-Ni25	$(4.08\pm2.04)\times10^{-5}$	151 0$\pm$20	3.5X1 0^{-6}	17
22	Egry 2	Ni	$(1.82\pm0.45)\times10^{-5}$	1490120	1. OX1O-5	26
23	Egry 4	Ni	$(1.82\pm0.45)\times10^{-5}$	1490$\pm$20	1.0x10^{-5}	26
24	Flemings 5	Ni	$(1.82\pm0.45)\times10^{-5}$	1490f 20	1. OX10"5	26
25	Herlach 2	Ni99.4-C0.6	$(1.82\pm0.45)\times10^{-5}$	1490$\pm$20	1. OX1O-5	26
26	Bayuzick 1	Zr	Not measured			

Table 2. A comparison of the experimental and theoretical evaporation rates of the metals and alloys used in TEMPUS.

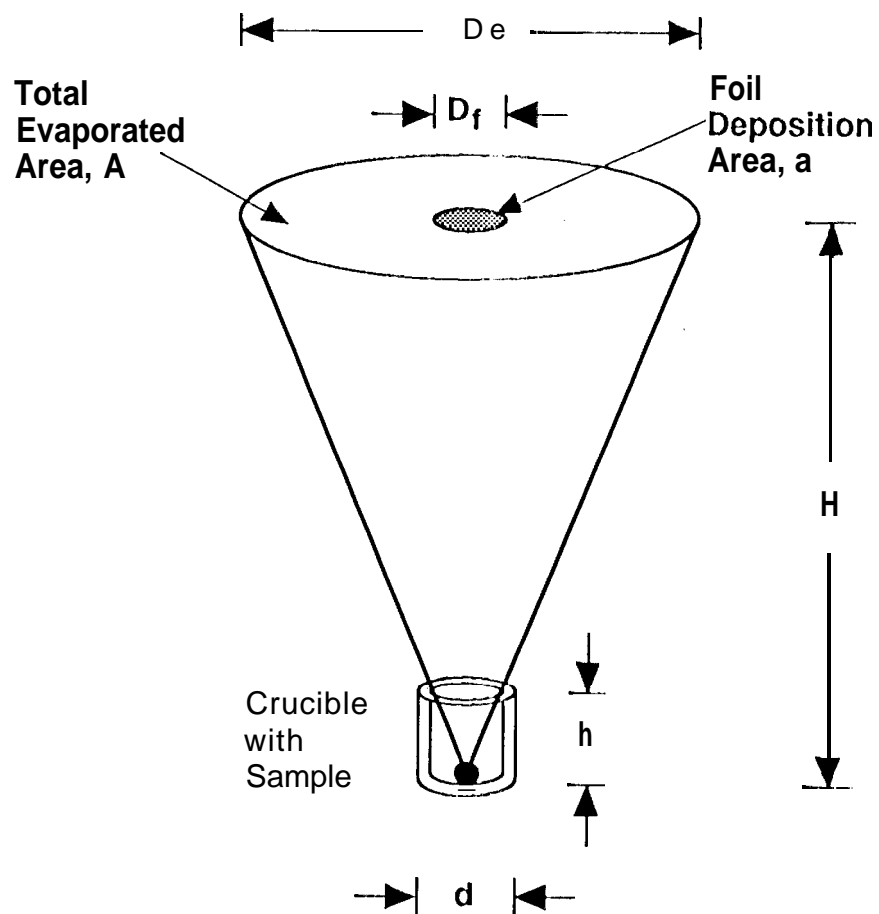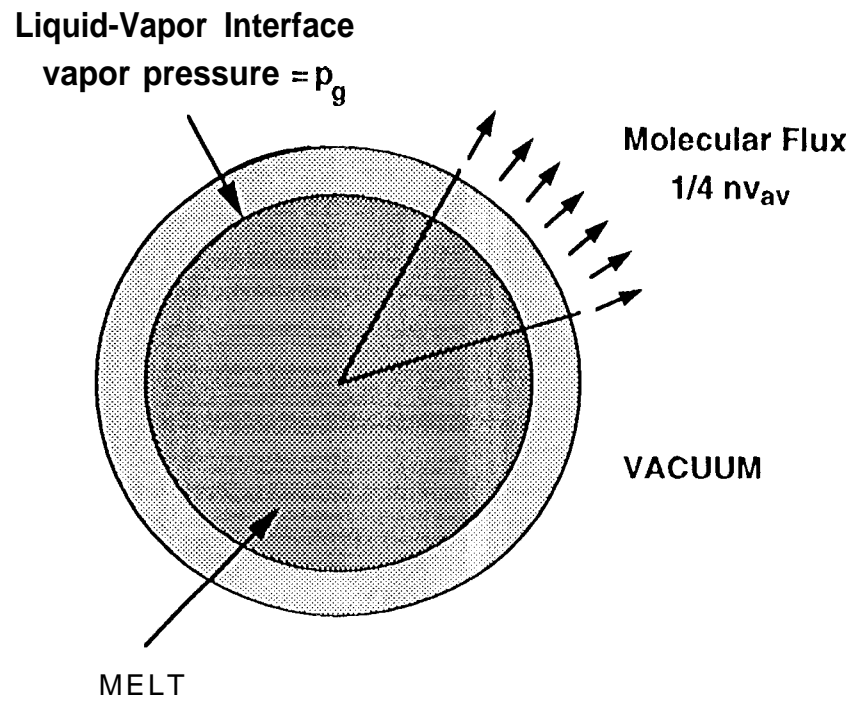| FO#	FO	Material Sample	Expt. Evaporation Rate $(g/cm^2.s)$	Temperature $(°C)$	Theo. Evap. Rate$(g/cm^2.s)$
2	Urban 1	Al60-Cu34-Fe6	$(3.16\pm1.58)\times10$-7	965 ± 10	5.78×10^{-7}
3	Egry 1	Au	$(5.22\pm1.30)\times10^{-6}$	1124 ± 10	2.59×10^{-7}
4	Egry 3	Au	$(5.22\ H.36)\times10^{-6}$	1124 ± 10	2.59×10^{-7}
5	Flemings 1	Ni75-Sn25	Spitted (in E.3N crucible)	1275 ± 10	1.73×10^{-5}
			$(3.56\pm1.78)\times10^{-6}$ (in AO crucible)	1285 ± 10	2.30×10^{-5}
6	Szekely 1	Au56-CU44	$(1.04\pm0.26)\times10^{-6}$	$1075\pm1o$	4.07×10-6
7	Flemings 3	Ni67.5-Sn32.5	$(1.31\pm0.65)\times10^{-6}$	1192 ± 10	2.19×10^{-6}
8	Szekely 4	Cu	$(3.46\pm0.86)\times10^{-5}$	1123 ± 10	1.16×10^{-5}
9	Herlach 3	Ni79-Si21	$(4.06\pm2.03)\times10^{-7}$	1224 ± 10	$3.0lX10$-7
10	Fecht 1	Zr64-Ni36	$(2.21\pm0.55)\times10^{-8}$	1090 ± 1 o	8.13×10^{-8}
11	Fecht 2	Zr76-Fe24	$(1.00\pm0.50)\times10^{-7}$	10183-15	4.21×10^{-9}
12	Johnson 4	Ni59.5-Nb40.5	$(3.72\pm1.86)\times10^{-6}$	1370 ± 15	4.74×10-6
			$2.27\pm0.56)\times10^{-7}$	1225 ± 10	2.48×10-7
13	Bayuzick 2	Zr	Not measured		
14	Urban3	Al65-Cu25-Co10	$(1.14\pm0.57)\times10^{-6}$	1050 ± 10	3.12×10^{-6}
15	Szekely 3	Au56-Cu44	$(1.04\pm0.26)\times10^{-6}$	1075 ± 10	$4.07X10'$-6
16	Flemings 4	Ni67.5-Sn32.5	$(1.31\pm0.65)\times10^{-6}$	1192 ± 10	2.19×10^{-6}
17	Johnson 3	Zr76-Ni24	$(7.24\pm1.81)\times10^{-8}$	1100 ± 15	9.23×10^{-9}
			$<(4.78\ 11.20)\times10^{-9}$	1055 ± 10	$3.70X10$-9
18	Fecht 3	Zr78.5-Co21.5	$<(2.76\pm1.38)\times10^{-9}$	1082 ± 15	$4.47X10^{-8}$
19	Urban 2	Al67-Cu21-Co12	$(4.88\pm2.44)\times10$-5	1320 ± 15	7.89×10^{-4}
			$(7.28\pm3.64)\times10^{-7}$	$109O*10$	6.85×10^{-6}
20	Flemings 2	Ni75-Sn25	Spitted (in BN crucible)	1275 ± 10	1.73×10^{-5}
			$(3.56\pm1.78)\times10^{-6}$ (in AO crucible)	1285 ± 10	2.30×10^{-5}
21	Herlach 1	Fe75-Ni25	$(4.08\pm2.04)\times10^{-5}$	1510 ± 20	2.88×10^{-4}
22	Egry 2	Ni	$(1.82\pm0.45)\times10^{-5}$	1490 ± 20	7.81×10^{-5}
23	Egry 4	Ni	$(1.82\pm0.45)\times10^{5}$	1490 ± 20	7.81×10^{-5}
24	Flemings 5	Ni	$(1.82\pm0.45)\times10^{5}$	1490 ± 20	7.81×10-5
25	Herlach 2	Ni99.4-C0.6	$(1.82\pm0.45)\times10^{-5}$	$1490\sim20$	9.28×10^{-5}
26	Bayuzick 1	Zr	Not measured		
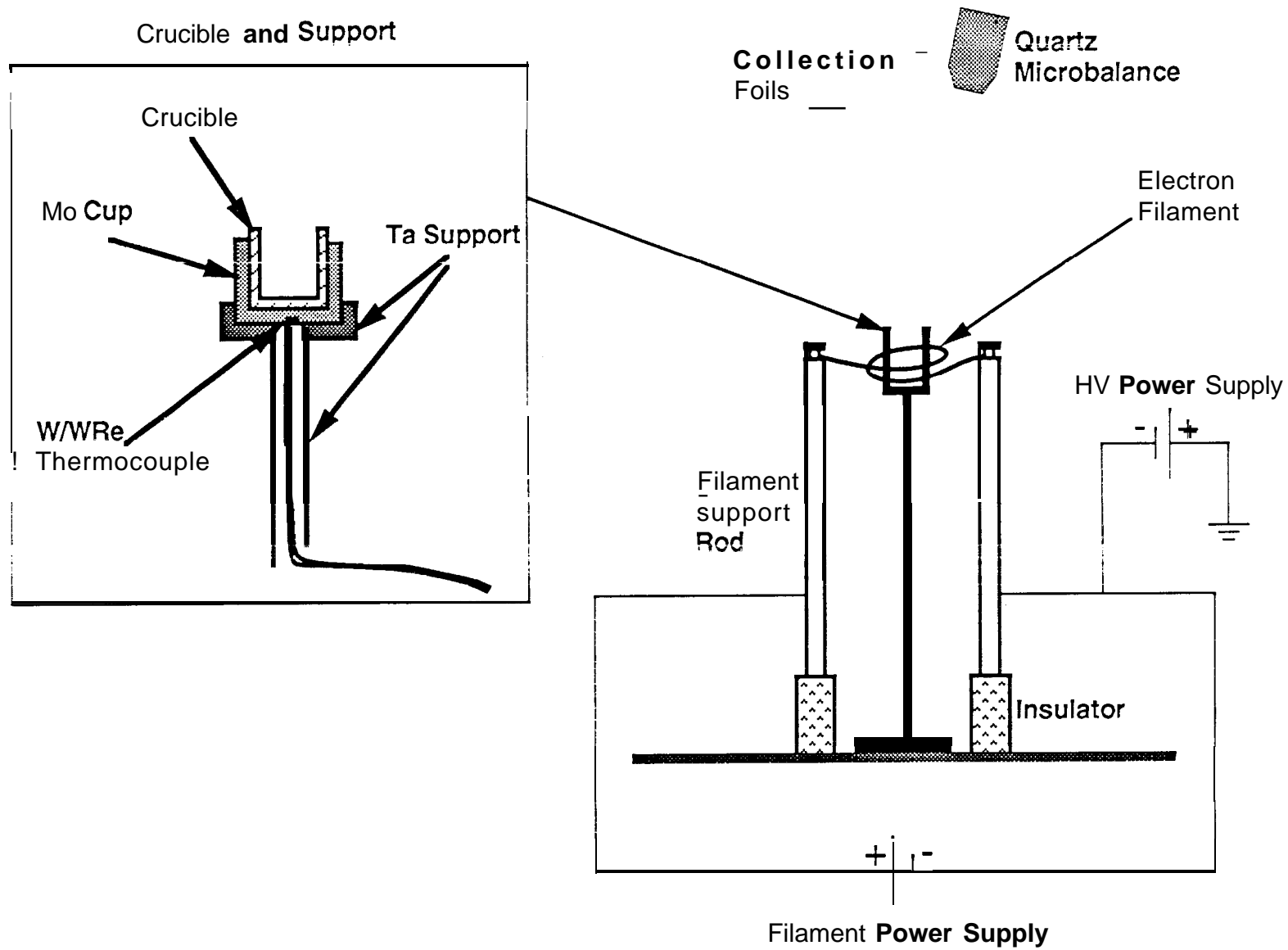
Fig 1. Apparatus for Evaporation Rate Measurements

Fig 2. Geometry used for obtaining the evaporated area in the calculation of evaporation rate from film thickness measurements

Liquid-Vapor Interface

vapor pressure $= p_g$

Molecular Flux

$1/4\ nv_{av}$

VACUUM

MELT

Fig. 3. Simple Model Showing an Evaporating Sphere.